Atomistic simulations of helium, hydrogen, and self-interstitial diffusion inside dislocation cores in tungsten

Mathew, Nithin
Perez, Danny
Martinez Saez, Enrique

To be published in: Nuclear Fusion

DOI to publisher's version: 10.1088/1741-4326/ab6061

Atomistic Simulations of Helium, Hydrogen, and Self-interstitial Diffusion inside Dislocation Cores in Tungsten

Nithin Mathew, Danny Perez, Enrique Martinez

Theoretical Division T-1, Los Alamos National Laboratory, Los Alamos, NM, 87545

Abstract

Tritium retention and microstructural modifications due to helium accumulation are two of the main concerns regarding plasma-facing materials in fusion applications. Crystal defects in Tungsten (W), such as grain boundaries and dislocations, can serve as traps or channels for diffusion of Hydrogen (H) and Helium (He), and, as such, can affect the transport of these species. In this work, we study the diffusion of Hydrogen, Helium and self-interstitial atoms (SIA) inside screw and edge dislocations in W using molecular dynamics simulations. Stable sites for interstitials in dislocations are identified using a free-volume analysis and energy barriers for diffusion are predicted using a combination of the Nudged Elastic Band (NEB) method and finite temperature molecular dynamics simulations. Overall, the simulations predict higher energetic barriers for He and H diffusion in both screw and edge dislocations compared to the bulk. However, the diffusion mechanism in both dislocations are shown to differ: simulations predict that interstitials are constrained to move in short channels inside the edge dislocation core so that long-range diffusion along the dislocation line happens only with the motion of the dislocation. In contrast, one-dimensional diffusion of the interstitial along the dislocation core, independent of dislocation motion, is observed for screw dislocations.

1. Introduction

Tungsten (W) is the leading candidate for divertor material in future nuclear reactors such as the International Thermonuclear Experimental Reactor (ITER[1]).[1,2] This choice is motivated by the high melting point, high thermal conductivity, and high resistance to sputtering and neutron damage. Tritium management, for both safety and economic reasons, will be crucial for the acceptance of fusion as an environmentally benign power source. Retention of Tritium in plasma facing materials (PFM) is understood as a primary concern for next step fusion devices fueled with mixtures of Deuterium (D) and Tritium (T), with critical implications for in-vessel component design, material selection, operational schedule and safety.[3–5] Tritium inventory control is crucial to reduce tritium outgassing and thus to minimize personnel exposure during venting of the torus for maintenance. Independently of safety limits, control of the in-vessel tritium inventory is also necessary to avoid exhausting the available tritium supply.[6–8]

Further, energetic hydrogenic species and Helium (He) ash from the fusion reactions collide with the W divertor, resulting in a variety of microstructural changes in the PFM. Exposure to pure He or mixed He-Hydrogen (H) particles, even below the threshold energy for sputtering, leads to the formation of a variety of surface defects which include nanoscale features generally referred to as "fuzz", micron-sized holes, micro-cracks, and mixture of fuzz and holes referred to as "coral"[9–11]. A variety of mechanisms have been proposed for the formation of He fuzz and H

[1] https://www.iter.org/

blisters and these are discussed in depth in ref. [11] and references therein. Such microstructures might promote the emission of high-Z dust into the plasma leading to abnormal operation failure. In addition, occasional formation of H blisters has also been reported for W, which has been linked to the retention of H by voids and vacancies. Formation of H blisters is however inhibited by the presence of He-induced fuzz.

Retention of H and He is thus a leading concern for the use of W divertors and first wall material. Grain boundaries[12–18] and dislocations,[19] along with vacancies and vacancy clusters, can serve as traps for H and He and result in their retention in the divertor. In turn, H and He act as pinning points for dislocations, resulting in hardening. Multiple simulation studies using Density Functional Theory (DFT)[20–23], classical Molecular Dynamics (MD)[19,24–26], and multi-scale methods[27] have been undertaken to study the role of dislocations in H and He retention and He bubble growth. DFT calculations[20] predict that He binds more strongly to dislocations compared to H. It has also been shown using DFT calculations[20] that H/He have stronger affinity for edge dislocations compared to screw dislocations and that a single screw dislocation can retain up to six H atoms[28] per unit dislocation length without undergoing any transformation. A recent DFT[22] study showed that H binding can result in spreading of the screw dislocation core. Theoretical studies[23,28] have also suggested that dislocation networks can play an important role in transporting H through the bulk to the surface. In addition, experimental studies[29] have found that evolution of dislocation density with temperature, in self-irradiated W, was correlated with D retention. However, a detailed understanding of interstitial-transport along dislocations and grain boundaries and associated energetic barriers is still developing.

In this manuscript we present classical MD predictions for energy barriers of H, He, and self-interstitial atoms (SIA) migration in edge and screw dislocation cores. We use a free-volume analysis to identify stable sites for interstitials inside the dislocation cores and corroborate the results of this analysis using binding energy calculations. Energy barriers for interstitial migration are calculated using a combination of Nudged Elastic Band[30,31] (NEB) method and finite temperature MD simulations. Our simulations show the presence of inter-connected regions of maximum free-volume (channels) inside the edge dislocation core, aligned at an angle to the dislocation line direction. The interstitial is constrained to move inside these channels and exhibits 1D diffusion confined to the glide plane. This effect is similar to the "conjugate channeling" motion of carbon interstitials previously predicted in BCC-Iron (Fe) using MD simulations.[32] Our analysis also identify paths for 1D (pipe) diffusion of H and He interstitials along the line of screw dislocations, albeit with higher energy barriers than bulk. A path with extremely low barrier for 1D diffusion of SIAs is predicted inside the screw dislocation but not in the edge dislocation.

2. Methods

MD simulations of the W-He-H system were performed using a recently developed EAM interatomic potential.[33] In this potential the W-W interaction is unchanged from the EAM-2 potential developed by Marinica et al.[34], which provides good predictions of mechanical properties of W.[35] Parametrization of the W-H and H-H interactions are described in detail by

Wang et al.[33] The potential of Juslin et al[36] was used for W-He interaction and the He-He interaction was described by the Beck potential[37] modified at short distances by Morishita et al.[38] Recent DFT simulations[39] have shown that the W-He-H potential developed by Wang et al is more accurate in reproducing DFT predictions of interactions between H and He-Vacancy complexes compared to the Bond Order Potential (BOP) developed by Juslin et al.[40] Moreover, point defect properties of H, such as formation energies and migration energy are well predicted by this potential.[33] In addition, interaction between H and vacancy clusters predicted by this potential is in better agreement with DFT results compared to predictions by all the other W-H potentials in literature (see Table 6 in [33]). These favorable properties, combined with the 3× speed-up compared to BOP, makes the EAM potential by Wang et al. an ideal choice for large-scale MD simulations of W-He-H ternary systems with dislocations. A timestep of 1 fs was used for simulations where only W is present; this value was decreased to 0.5 fs when H or He was added. Coordinates were saved at a frequency of 1 ps for subsequent analysis. All simulations were performed using the LAMMPS MD software.[41] Analysis of the simulations were performed using the Common Neighbor Analysis (CNA)[42], Dislocation Extraction Analysis (DXA), and Wigner-Seitz analysis as implemented in OVITO.[43–45] NEB calculations were performed using the implementation in LAMMPS with the forces converged to at least 0.03 eVA^{-1}.

Initially pristine simulation cells of W were created with the cartesian x, y, and z directions oriented along [-111], [1-12], and [110] crystallographic directions, respectively. Dislocations were inserted into this cell using the Volterra elastic field as implemented in the ATOMSK[46] software. For both screw and edge dislocations, simulation cells were created to ensure periodicity along the [-111] and [1-12] directions. Calculations with the edge dislocation was performed using a simulation box of size 156.446×15.374×159.889 Å and that for screw dislocations were of size 28.426×138.399×137.739 Å. Energy minimization of these simulation cells with dislocations were performed to ensure that initial configurations had stresses close to zero and traction-free surfaces. A vacuum padding of 50 Å was used in the [110] direction with two layers of atoms held fixed at the z=0 and z=$\max(z)$ in all simulations to ensure constant volume conditions.

3. Results and Discussion

3.1. Analysis of dislocation core structures

The initial focus was to identify favorable binding sites for H, He, and SIAs in the cores of edge and screw dislocations. For this purpose, a free-volume analysis of the dislocation cores was performed using the methodology described in Ref. [47]. In this analysis, a repulsive pairwise potential is used to model the interaction between the interstitial and the host lattice. In effect, this geometry analysis yields a parameter, $S(r)$, which provides an estimate of the local free-volume around any point in the host lattice. Figure 1 shows results of this analysis, where the blue regions show 3D contours corresponding to large $S(r)$ around the edge and screw dislocation cores. From an energetic perspective, interstitial atoms would likely favor those sites with largest free-volume.

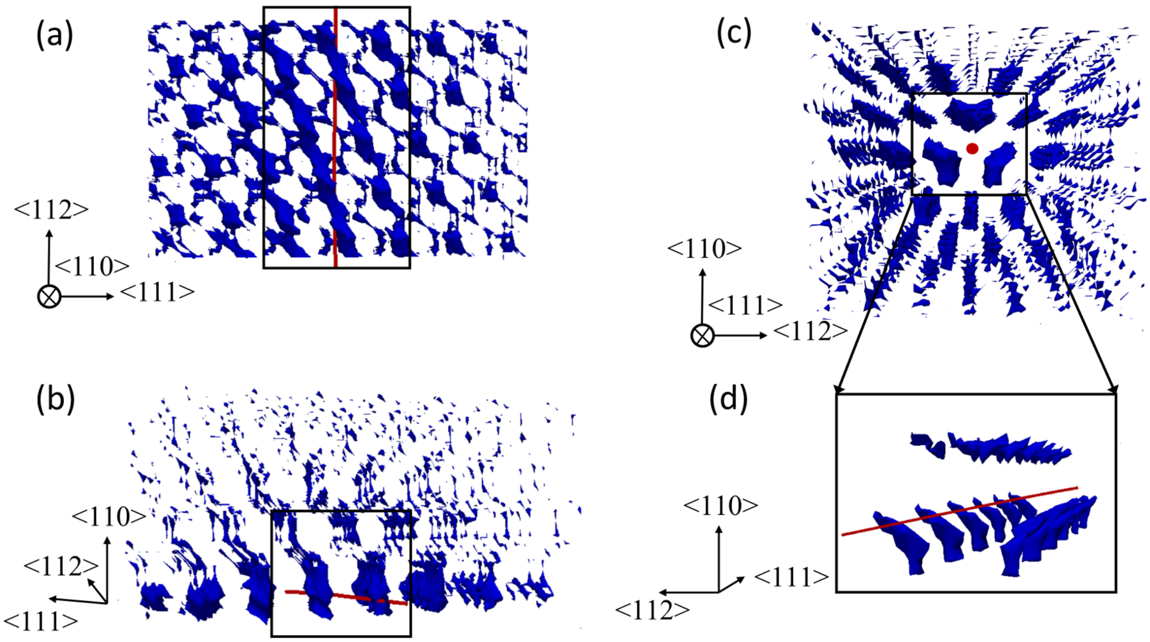

Figure 1: Contours of constant free-volume in the static equilibrium structure of dislocation cores at zero pressure. The contours are filtered to highlight the dislocation core region demarcated using black boxes. The dislocation line is shown using the red line. (a) edge dislocation viewed normal to the glide plane showing interconnected regions of large free-volume (channels) at an angle to the dislocation line direction (<112>) (b) edge dislocation viewed approximately normal to the channel (c) screw dislocation showing the nominally three-fold symmetry of the distribution of free-volume (d) zoom-in of the screw dislocation core showing that the regions of high free-volume are not connected along the dislocation line direction (<111>).

Evident from Figure 1(a) is the presence of interconnected regions of large free-volume resulting in linear 'channels' inside the core of the edge dislocation. Such interconnected regions are not present in the screw dislocation, as is evident from Figure 1(b). The distribution of free-volume suggests that interstitial atoms could undergo 1D diffusion in these channels in the edge dislocation, but such a mechanism may not be present in screw dislocations. Instead, these regions of high free-volume are present as disconnected 'lobes' with nominal 3-fold symmetry around the core of the screw dislocation. These lobes are arranged in a helical pattern running along the <111> direction. (Readers are also referred to a 2D projection of $S(r)$ on a mean-plane of the dislocation core shown in Figure 3.)

The conclusion from the free-volume analysis is corroborated by the binding energy calculations of the interstitials with the dislocation cores. The binding energy of the interstitial (X) with the dislocation was calculated using the following equation:

$$E_b = E_{disl-X} - E_{disl} - E_X^0 - E_X^f \quad (1)$$

Here E_b is the binding energy, E_{disl-X} is the minimized total potential energy of the simulation cell with the dislocation and the interstitial (at constant volume), E_{disl} is the minimized total potential energy of the simulation cell with only the dislocation, E_X^0 is the reference energy for the interstitial (which are taken as -0.0052, -2.3576, and -8.89998 eV for He, H, and the SIA respectively), and E_X^f is the formation energy, in the tetrahedral position for H/He interstitials and in the <111> crowdion configuration for the SIA, in the bulk W matrix. In this definition a negative value implies attractive interaction. Figure 2 shows the binding energy maps for edge (panels a-c) and screw (panels d-f) with the type of the interstitial specified on top right corner of each panel.

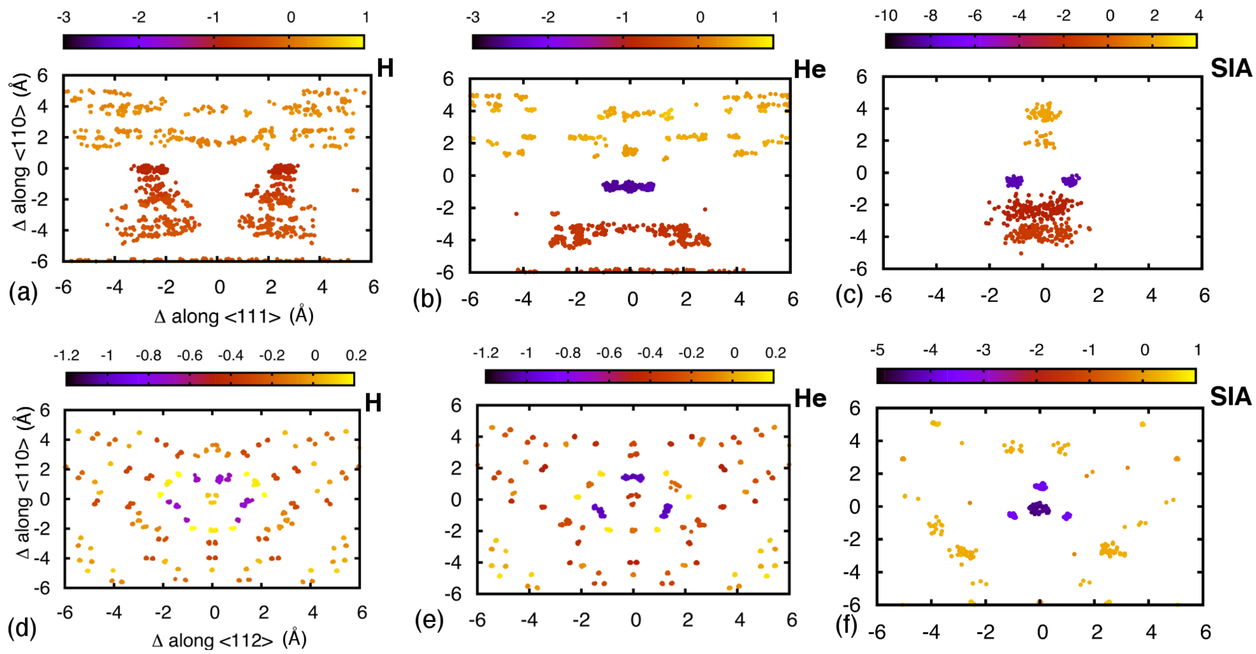

Figure 2: Maps of binding energy (eV) of H, He, and SIA atoms (ordered from left to right) with dislocation cores. (a-c) are for edge and (d-f) for screw dislocations with the type of interstitial specified at top right corner of each panel. All axes are from -6 to 6 Å and the core of the dislocation is located at (0,0) in all panels. Color bars (in units of eV) are above the respective panels.

In Figure 2, the core of the dislocation, whose position was extracted using DXA, is located at (0,0). A few interesting observations can be made from the figure. It is evident that all interstitials bind more strongly to edge dislocations compared to screw dislocations, consistent with existing DFT predictions.[20] For a given type of dislocation, the binding energy of the interstitials are ordered as SIA > He > H. Stronger binding of He to dislocations compared to H has also been predicted by DFT calculations.[20] Additionally, this potential predicts that H and SIA, unlike He, do not bind to the interior of the edge dislocation (as is evident from the empty region near (0,0) for panels a and c). We note that this conclusion for H is in contradiction to existing DFT calculations and calculations using the BOP and EAM potentials described in ref.[20] However, as we will discuss later, MD simulations with the current potential do predict that H interstitials and

SIA can remain in this interior region of edge dislocation at finite temperatures, indicating that they are entropically stabilized. The 3-fold symmetry of the screw dislocation core is present in panels d-f, corresponding to the regions of largest free-volume (denoted as 'B' position in ref. [21]) are indeed preferred binding sites for the H and He interstitial atoms in the screw dislocation. Also, it can be seen that SIA has a higher binding energy to the interior of the screw dislocation core compared to the lobes with largest free-volume. SIA binds strongly to edge and screw dislocation cores with E_b < -4 eV – this implies that SIA, which may form from trap mutation events during He-bubble growth near dislocations, will remain strongly bound to the dislocations.

3.2. Nudged Elastic Band Calculations

Following the identification of stable sites, we performed NEB calculations to determine the energy barrier for site-to-site migration of interstitials. Configurations for the end points were created by placing an interstitial atom at sites with maximum free-volume followed by energy-

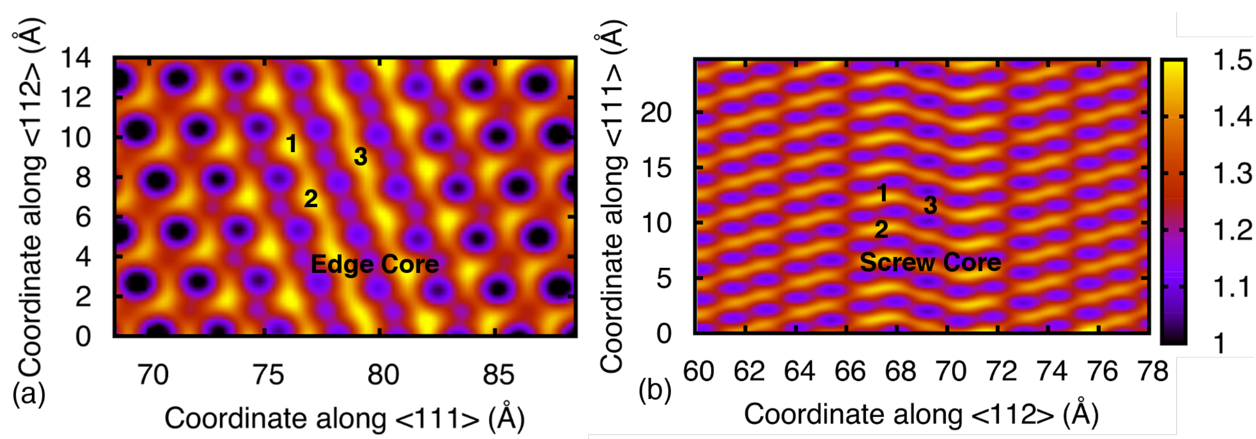

Figure 3: 2D projection of the contours of $S(r)$ (in units of Å) on the mean-plane of the dislocation core. (a) Edge dislocation (b) Screw dislocation. Numbers 1,2,3 are used to denote the sites with maximum free-volume where interstitials are positioned for NEB calculations.

minimization at fixed volume. Initial configurations for the intermediate images were created using linear interpolation between the atomic coordinates of the end points.

Figure 3 shows 2D projections of the $S(r)$ parameter on a mean-plane of the dislocation core with the location of initial/final configurations for NEB calculations denoted using numbers (1,2 and 3). The ‘channels’ in the core region of the edge dislocation are clearly visible in the figure. Also, these channels are finite and are oriented at an angle to the dislocation line, which lies along a <112> direction (the ordinate axis in Figure 3(a)). In-channel motion therefore cannot lead to long-range transport, unless the dislocation glides. The results of the NEB calculations for site-to-site hopping of He inside the edge dislocation core are shown in Figure 4.

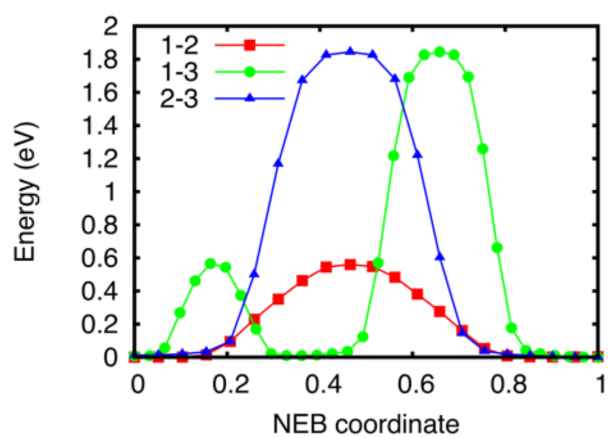

Figure 4: Energy of NEB replicas as a function of the NEB coordinate for site-to-site hopping of He inside the edge dislocation core.

The curve denoted as 1-2 in the figure shows the minimum energy pathway for site-to-site hopping of He within (along) the channel, with a predicted energy barrier of 0.56 eV. A much higher barrier of 1.84 eV is predicted for direct hopping from one channel to another (2-3). The curve denoted as '1-3', which is also for channel-to-channel hopping, shows two barriers: a smaller barrier of 0.56 eV for in-channel hopping from sites 1 to 2, followed by the larger barrier of 1.84 eV for channel-to-channel hopping from 2 to 3. As H is not stable in the interior of the edge dislocation core at 0 K (see discussion of Figure 2), we were not able to perform this analysis for those interstitials. An estimation of the barrier for H diffusion from finite temperature MD simulations in presented in Section 3.3.

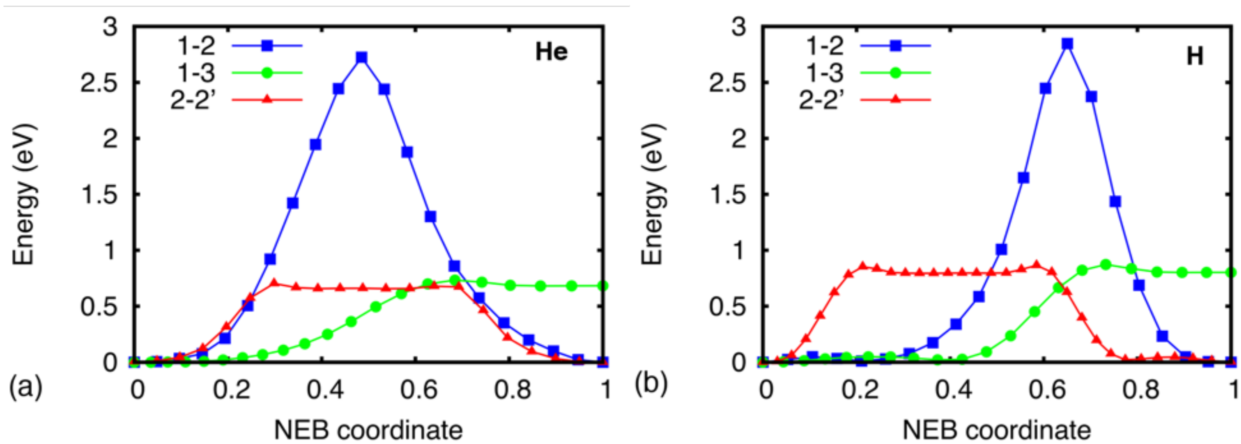

Figure 5: Energy of NEB replicas as a function of the NEB coordinate for site-to-site hopping of interstitials inside the screw dislocation core. (a) He and (b) H.

Figure 5 shows the results for NEB calculations for site-to-site hopping of He and H inside the screw dislocation core. Sites 1,2,3 are shown in Figure 3: sites 1 and 2 are located in the lobes with large free volume in the mean-plane of screw dislocation, site 2' is the symmetric equivalent of 2 located above the mean-plane and along the helix of the screw dislocation, and site 3 is situated in the interior, i.e. region close to (0,0) in Figures 2(d)-2(f). NEB calculations reveal that hopping from lobe-to-lobe (1-2) in the mean-plane has a high energetic barrier > 2.5 eV for both He and H. At the same time, lobe-to-lobe hopping along the helix of the screw dislocation (2-2') has relatively low barriers of 0.70 eV for He and 0.86 eV for H. In addition, it can be seen that He and H can move from the interior of the screw to the lobes (3-1) with very small barriers of 0.05 eV for He and 0.07 eV for H. Qualitatively, this agrees with previous DFT[23,28] calculations that have predicted energy barriers on between ≈0.07-0.1 eV for migration of H between meta-stable sites on screw dislocations. Based on these results, it can be deduced that diffusion of H and He along the core of the screw dislocation does not happen and lobe-to-lobe hopping along the helix of the screw dislocation core is the most probable mechanism for diffusion of H and He.

NEB calculations were also performed to obtain barriers for diffusion of SIAs. As SIA diffusion may occur by non-trivial rearrangement of the W atoms, we performed high temperature MD simulations with periodic quenching to obtain the stable neighboring configurations for the diffusing SIA. These simulations were performed using a simulation cell with a longer dislocation line (dimensions 85.481×138.399×137.739 Å and a vacuum of 30 Å) to prevent the migration of screw dislocation at high temperatures. Very fast diffusion of SIA along the screw dislocation core is predicted in our simulations at 1500 K. The SIA diffuses along the 'core' of the screw dislocation (denoted as 'A' position in ref. [21]) and not the lobes, in contrast to H and He. Figure 6(a) shows the trajectory of the diffusing SIA (bright yellow cloud) at 1500 K, superimposed on the binding energy map; Figure 6(b) shows the result of the NEB calculation for stable SIA sites along the line of the screw dislocation obtained from this trajectory.

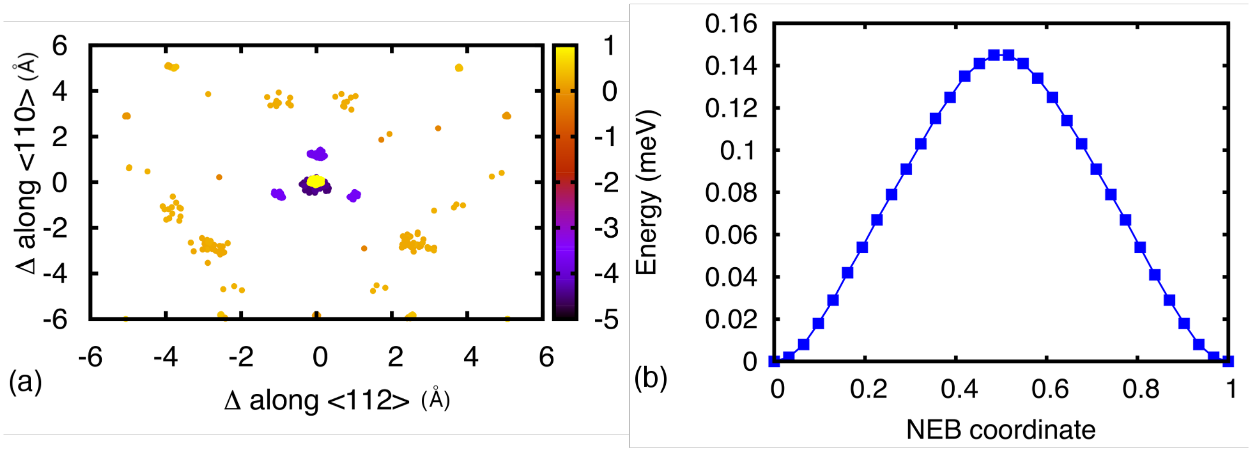

Figure 6: Diffusion of SIA in the screw dislocation. (a) Relative positions of SIA (bright yellow cloud) with respect to the screw dislocation core from finite temperature molecular dynamics simulations, at 1500 K, superimposed on the binding-energy map (in units of eV) (b) Energy of NEB replicas as a function of the NEB coordinate for hop of SIA along the screw dislocation line.

Our calculations predict an extremely small barrier of 0.14 meV for SIA diffusion along the line direction of the screw. Even though a barrier on the order of few meVs is expected, given that the dislocation line is oriented along <111>, the predicted barrier is much lower than the 17 meV barrier[48] predicted with this potential for SIA diffusion in the bulk. Upon examining the stable sites obtained from the high temperature runs, we see that SIA diffusion happens in effect by 1D migration of a kink along the dislocation line. A recent investigation of mobility of kinks on screw dislocations in BCC-Fe has revealed that their diffusivity scales linearly with temperature,[49] indicating a vanishing energy barrier. Atomistic calculations in BCC-Fe[50] have also predicted migration energy barriers <0.1 meV for kinks on screw dislocations. These findings agree qualitatively with our results. In contrast, no diffusion of SIA was observed along the line of edge dislocations despite multiple trials at 2000 K indicating high barriers for SIA diffusion along the edge dislocation.

3.3. Finite temperature molecular dynamics simulations of interstitial H/He in edge/screw dislocations

Although binding energy calculations showed an exclusion region in the interior of the edge dislocation core for H, finite temperature MD simulations revealed that H can reside in the channel, possibly being entropically stabilized, and undergo 1D diffusion along the channel on the glide plane. Therefore, we performed a suite of MD simulations from 850 K – 1000 K to estimate the energetic barrier for diffusion of H along the edge dislocation. No channel-to-channel hopping of H (site 2-3 in Figure 3a) was observed in any of our simulations. The results showed that H may occasionally unbind from the edge dislocation at T > 850 K; therefore, multiple MD runs of length 6 ns with different initial conditions were performed and all trajectories with unbounded H were discarded. The position of H interstitial was output every 1 ps to calculate the mean-squared displacement (MSD) as a function of time. Averaging was performed over all time origins up to half of the total simulation time to ensure equal weighting of all time origins. Averaging of $\langle MSD \rangle$ was also performed over 7 different trials, resulting in a total simulation time of 42 ns at each temperature. The $\langle MSD \rangle$ at these temperatures were found to saturate within ≈1 ns to a value close to the squared length of the channels, indicating that diffusion of H is constrained. The short-time diffusion coefficient (D) was calculated using the Einstein relation, $D = \lim_{t\to\infty} \langle MSD \rangle / 2t$, by linear-regression of the $\langle MSD \rangle$ between 10 and 325 ps. Figure 7(a) shows the linear regime of the $MSD(t)$ for in-channel diffusion and Figure 7(b) shows the natural logarithm of D (in units of Å^{2}ps^{-1}) as a function of $1/T$. Again, it should be stressed that this quantity only measures diffusion in a single channel, which has a finite length. It is therefore only valid to describe motion over short timescales and does not characterize long-range transport. The estimated energy barrier from the slope of Figure 7(b) is 0.49$\pm$0.07 eV, which is close to the lowest barrier predicted for He diffusion in edge dislocation.

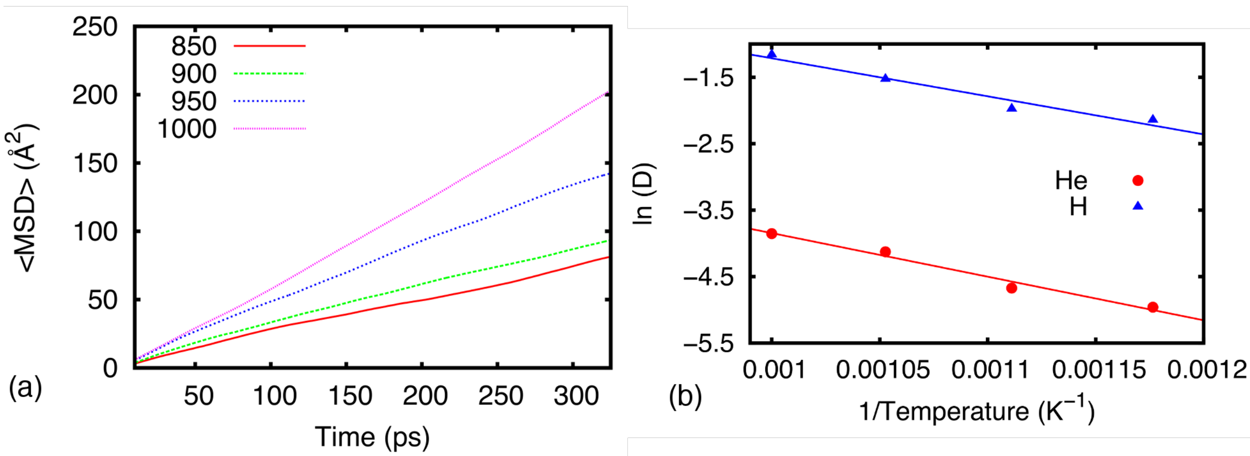

Figure 7: Diffusion of H/He inside the edge dislocation (a) Average mean-squared displacement as a function of time for H (b) Natural logarithm of diffusion coefficient (D in units of Å^{2}ps^{-1}) as a function of inverse temperature for H and He.

We also performed finite temperature MD simulations of He diffusion in the edge dislocation. Both set of simulations predicted a correlated motion of He/H with the motion of the edge dislocation. To ascertain the energy barrier for diffusion of interstitial associated with the motion of the edge dislocation, we performed NEB calculations between configurations in which the edge dislocation with the interstitial moved by a burgers vector. These calculations provided a barrier of 0.56 eV for He and predicted a process in which the dislocation moves, carrying the channels with it, and the He hops within the channel. This indicates that the diffusion of the interstitial is limited by the barrier for site-to-site hopping within the channel (1-2 in Figure 3a). The energy barrier for diffusion of He in edge dislocation was also estimated from the finite temperature MD runs. Figure 7(b) shows the natural logarithm of diffusion coefficient (D in units of Å^{2}ps^{-1}) as a function of inverse temperature obtained from linear-regression of the $\langle MSD \rangle$

between 10 and 650 ps for He. In this case, averaging of $\langle MSD \rangle$ was performed over 9 different trials of 6 ns each, resulting in a total simulation time of 54 ns at each temperature. The estimated barrier for He is 0.57$\pm$0.06 eV, which is in very good agreement with the value obtained from NEB calculations. The pre-factors estimated for diffusivity in edge dislocation (in units m^2s^{-1}) are 9.1E-07 for H and 1.5E-07 for He. All values for the energy barriers (in eV) predicted by our calculations (both NEB and MD) are compared to existing values in the literature for bulk diffusion in Table 1.

System	E_a^H	E_a^{He}	E_a^{SIA}
Bulk	0.22[33], 0.4[51]	0.21[36]	0.017[48]
Edge dislocation	0.49$\pm$0.07*, 0.17[21]	0.56 (0.57$\pm$0.06*)	--
Screw dislocation	0.86	0.70	0.00014

*Table 1: Predicted energy barriers (in eV) for diffusion of H, He and, SIA in W compared to experimental and computational values available in the literature. The symbol * denotes values predicted from finite temperature MD simulations in our studies.*

Finite temperature MD was also performed to further analyze the diffusion mechanisms for He/H in the screw dislocation. Figures 8(a) and 8(b) show representative MD trajectories of He (1100 K) and H (1200K) diffusion respectively, on screw dislocations superimposed on the binding-energy maps. Both trajectories are 1.5 ns long. The bright yellow cloud in both figures shows the relative position of the interstitial with respect to the dislocation core. The core is located at (0,0).

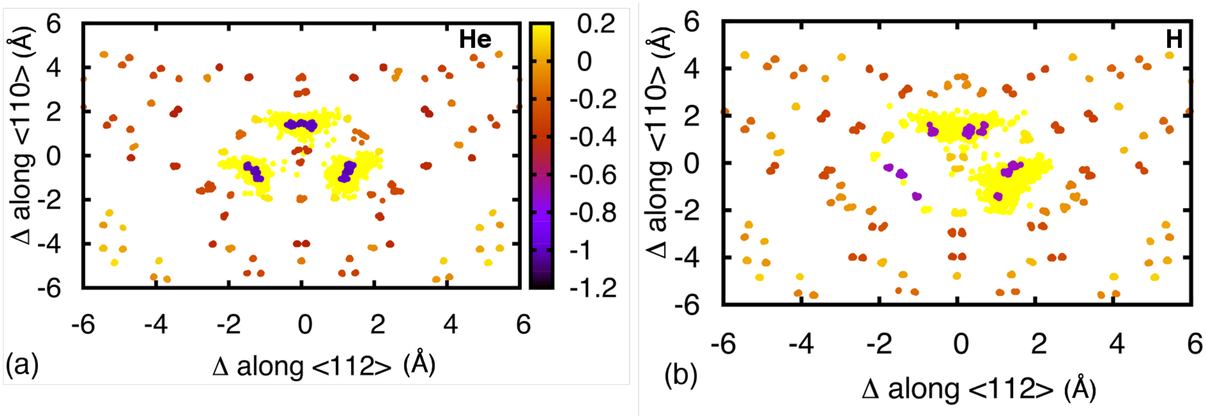

Figure 8: Relative positions of interstitials (bright yellow cloud) with respect to the screw dislocation core from finite temperature molecular dynamics simulations superimposed on the binding-energy map (in units of eV). (a) He at 1100 K (b) H at 1200 K

Evidently, both He and H interstitials remain in the 3-fold lobes for most of the trajectory with occasional hops between them. This confirms the mechanism predicted by our static calculations for diffusion of He and H in the screw dislocation core.

In summary, our calculations predict slower diffusion of H/He interstitials along screw and edge dislocations compared to the bulk. 1D diffusion of H/He along screw dislocation lines happens through migration between lobes of large free-volume. This enables true long-range transport of He and H along the line direction even if the dislocation remains fixed, albeit at a lower rate than in the bulk. That being said, dislocation-mediated transport could still play an important role, as H and He both strongly bind to the dislocation. Hence, once trapped, motion mostly occurs along the line, until unbinding occurs on even longer timescales. In the case of the edge dislocation, He/H transport is easiest inside 1D channels of large free-volume that form at an angle to the dislocation line. Since the channels have a finite length, this mechanism does not allow for long-range motion on its own. Three possibilities remain for He/H transport in the edge dislocation: i) the dislocation glides, carrying the channels with it; this allows for the H/He atoms to move, but only by an amount that is proportional to the net displacement of the dislocation; ii) long-range motion follows from hops between channels; this enables long-range motion in a sessile edge dislocation albeit with a very high barrier; iii) unbinding occurs, and the transport occurs in the bulk; this again entails a very high barrier. These high barriers for inter-channel hopping and/or unbinding limit the efficiency of clustering by transport along the dislocation line. Hence, the formation of He/H bubbles at the core of an edge dislocation will mainly result from migration in bulk and subsequent reaction at the core. The channels will still be present under stress and therefore external solicitations do not seem to qualitatively change this conclusion. SIAs can undergo very fast diffusion with negligible barrier along the core region of screw dislocation. No diffusion of SIAs along the core of edge dislocations were predicted by MD simulations even at 2000 K. Thus, our results predict that high dislocation densities may slow down transport of He/H transport while enhancing SIA transport. Impeded transport of small He clusters near symmetric tilt GBs in W have been reported previously[16,18] and this is in qualitative agreement with our findings. These studies indicate that defects such as GBs and dislocations can trap and slow down He/H transport in W, leading to increased retention.

Our results for H diffusion in edge dislocation core is in contrast to existing MD calculations[21] (Table 1), albeit with a different H-W interatomic potential, which predicted a lower barrier compared to bulk. The origins of this difference, which very likely results from the different parametrizations H-W interactions, is unclear. We also note that studies using path-integral MD[52] and quantum mechanically informed kinetic Monte-Carlo simulations[53] in BCC-Fe have predicted slow diffusion of H along screw and edge dislocations compared to the bulk and our results are in qualitative agreement with these. Although the migration barriers may change for different parametrizations of the W-He-H interactions, the mechanisms that we have elucidated, such as the in-channel migration in edge and lobe-to-lobe migration in screw are expected to be present in other W-He-H potentials using the same underlying W-W interaction (such as in [54]).

4. Conclusions

Molecular dynamics simulations were performed to study the migration of H, He, and SIA along edge and screw dislocations in W. Stable sites for interstitials are predicted using a free-volume analysis of the dislocation cores in conjunction with binding energy calculations. Nudged Elastic Band calculations reveal that the preferred path for H and He migration along the screw dislocation is along lobes of maximum free-volume which exist in a 3-fold symmetric fashion about the <111> line direction. Migration energy for diffusion on this path for H/He is approximately 3-4 times the value in bulk. In contrast a different mechanism, with negligible barrier (0.14 meV) is predicted for migration of SIA on the screw dislocation. Migration of H/He inside edge dislocations is predicted to happen inside 1D channels of high free-volume, at an angle to the dislocation line, with an energy barrier that is approximately 2-3 times the value in bulk. Symmetry constraints dictate that this transport in edge dislocation is limited in length unless the edge dislocation itself moves. All mechanisms predicted by the static/NEB calculations, such as lobe-to-lobe/core diffusion along the screw dislocation and hopping between sites inside the channels in the edge dislocation, are confirmed by finite temperature molecular dynamics simulations.

Acknowledgements

Authors gratefully acknowledge support from the U.S. DOE, Office of Science, Office of Fusion Energy Sciences, and Office of Advanced Scientific Computing Research through the Scientific Discovery through Advanced Computing (SciDAC) project on Plasma-Surface Interactions (award no. DE-SC0008875). Computations were performed at Edison and Cori clusters at the National Energy Research Scientific Computing Center (NERSC), a U.S. Department of Energy Office of Science User Facility operated under Contract No. DE-AC02-05CH11231, and the Darwin Computing Cluster at Los Alamos National Laboratory. Los Alamos National Laboratory is operated by Triad National Security, LLC, for the National Nuclear Security Administration of U.S. Department of Energy (Contract No. 89233218CNA000001). This manuscript has been assigned LA-UR-19-28989.

References:

1. Aymar R. ITER overview. Fusion Eng Des. 1997;36:9–21.

2. Causey R, Wilson K, Venhaus T, Wampler WR. Tritium retention in tungsten exposed to intense fluxes of 100 eV tritons. J Nucl Mater. 1999;266:467–71.

3. Federici G, Wu CH, Esser B. Tritium retention in plasma facing components for NET/ITER fusion devices. Fusion Eng Des. 1991;16:393–405.

4. Causet RA, Venhaus TJ. The Use of Tungsten in Fusion Reactors: A Review of the Hydrogen Retention and Migration Properties. Phys Scr. 2001;T94:9.

5. Zakharov AP, Gorodetsky AE, Alimov VK, Kanashenko SL, Markin AV. Hydrogen retention in plasma-facing materials and its consequences on tokamak operation. J Nucl Mater. North-Holland; 1997;241–243:52–67.

6. Federici G, Brooks JN, Iseli M, Wu CH. In-Vessel Tritium Retention and Removal in ITER-FEAT. Phys Scr. 2001;T91:76–83.

7. Federici G, Skinner CH, Brooks JN, Coad JP, Grisolia C, Haasz AA, et al. Plasma-material interactions in current tokamaks and their implications for next step fusion reactors. Nucl Fusion. 2001;41:1967–2137.

8. Alimov VK, Roth J. Hydrogen isotope retention in plasma-facing materials: review of recent experimental results. Phys Scr. 2007;T128:6–13.

9. Nishijima D, Ye MY, Ohno N, Takamura S. Incident ion energy dependence of bubble formation on tungsten surface with low energy and high flux helium plasma irradiation. J Nucl Mater. 2003;313–316:97–101.

10. Nishijima D, Ye MY, Ohno N, Takamura S. Formation mechanism of bubbles and holes on tungsten surface with low-energy and high-flux helium plasma irradiation in NAGDIS-II. J Nucl Mater. 2004;329–333:1029–33.

11. Hammond KD. Helium, hydrogen, and fuzz in plasma-facing materials. Mater Res Express. 2017;4.

12. Liu X-Y, Uberuaga BP, Perez D, Voter AF. New helium bubble growth mode at a symmetric grain-boundary in tungsten: accelerated molecular dynamics study. Mater Res Lett. 2018;6:522–30.

13. Piaggi PM, Bringa EM, Pasianot RC, Gordillo N, Panizo-Laiz M, del Río J, et al. Hydrogen diffusion and trapping in nanocrystalline tungsten. J Nucl Mater. 2015;458:233–9.

14. González C, Panizo-Laiz M, Gordillo N, Guerrero CL, Tejado E, Munnik F, et al. H trapping and mobility in nanostructured tungsten grain boundaries: a combined experimental and theoretical approach. Nucl Fusion. 2015;55:113009.

15. Valles G, Panizo-Laiz M, González C, Martin-Bragado I, González-Arrabal R, Gordillo N, et al. Influence of grain boundaries on the radiation-induced defects and hydrogen in nanostructured and coarse-grained tungsten. Acta Mater. Pergamon; 2017;122:277–86.

16. Yang Z, Hu L, Maroudas D, Hammond KD. Helium segregation and transport behavior near 〈100〉 and 〈110〉 symmetric tilt grain boundaries in tungsten. J Appl Phys. 2018;123.

17. Hu L, Hammond KD, Wirth BD, Maroudas D. Dynamics of small mobile helium clusters near a symmetric tilt grain boundary of plasma-exposed tungsten. Fusion Sci Technol. 2017;71:36–51.

18. Yang Z, Hammond KD. Helium in-plane migration behavior on ⟨1 0 0⟩ symmetric tilt grain

boundaries in tungsten. J PhysCondens Matter. 2018;30:325002.

19. Smirnov RD, Krasheninnikov SI. Stress induced hydrogen self trapping in tungsten. Nucl Fusion. 2018;58:126016.

20. Bakaev A, Grigorev P, Terentyev D, Bakaeva A, Zhurkin EE, Mastrikov YA. Trapping of hydrogen and helium at dislocations in tungsten: An ab initio study. Nucl Fusion. 2017;57.

21. Grigorev P, Terentyev D, Bonny G, Zhurkin EE, Van Oost G, Noterdaeme JM. Interaction of hydrogen with dislocations in tungsten: An atomistic study. J Nucl Mater. Elsevier B.V; 2015;465:364–72.

22. Wang Y, Wang X, Wu X, Li Q, Li C, Shu G, et al. Hydrogen distribution induced screw dislocation core spreading in tungsten. J Nucl Mater. 2019;

23. Dubinko VI, Grigorev P, Bakaev A, Terentyev D, van Oost G, Gao F, et al. Dislocation mechanism of deuterium retention in tungsten under plasma implantation. J Phys Condens Matter. 2014;26:395001.

24. Xie H, Xu K, Lu GH, Yu T, Yin F. Trapping of hydrogen and helium at an {110}<111> edge dislocation in tungsten. J Nucl Mater. North-Holland; 2017;484:270–5.

25. Xie H, Xu K, Lu G-H, Yu T, Yin F. Dislocation climbing mechanism for helium bubble growth in tungsten. Scr Mater. Pergamon; 2018;147:98–102.

26. Gao N, Cui MH, Setyawan W, Kurtz RJ. Loop-punching suppression induced by growth of helium bubble pair in tungsten. J Appl Phys. 2018;124:0–6.

27. De Backer A, Mason DR, Domain C, Nguyen-Manh D, Marinica MC, Ventelon L, et al. Multiscale modelling of the interaction of hydrogen with interstitial defects and dislocations in BCC tungsten. Nucl Fusion. 2018;58.

28. Terentyev D, Dubinko V, Bakaev A, Zayachuk Y, Van Renterghem W, Grigorev P. Dislocations mediate hydrogen retention in tungsten. Nucl Fusion. 2014;54.

29. Založnik A, Markelj S, Schwarz-Selinger T, Ciupiński Ł, Grzonka J, Vavpetič P, et al. The influence of the annealing temperature on deuterium retention in self-damaged tungsten. Phys Scr. 2016;T167:14031.

30. Henkelman G, Jónsson H. Improved tangent estimate in the nudged elastic band method for finding minimum energy paths and saddle points. J Chem Phys. 2000;113:9978–85.

31. Henkelman G, Uberuaga BP, Jónsson H. Climbing image nudged elastic band method for finding saddle points and minimum energy paths. J Chem Phys. 2000;113:9901–4.

32. Ishii A, Li J, Ogata S. “Conjugate Channeling” Effect in Dislocation Core Diffusion: Carbon Transport in Dislocated BCC Iron. PLoS One. 2013;8:1–7.

33. Wang LF, Shu X, Lu GH, Gao F. Embedded-atom method potential for modeling hydrogen and hydrogen-defect interaction in tungsten. J Phys Condens Matter. 2017;29.

34. Marinica MC, Ventelon L, Gilbert MR, Proville L, Dudarev SL, Marian J, et al. Interatomic potentials for modelling radiation defects and dislocations in tungsten. J Phys Condens Matter. 2013;25.

35. Bonny G, Terentyev D, Bakaev A, Grigorev P, Van Neck D. Many-body central force potentials for tungsten. Model Simul Mater Sci Eng. 2014;22.

36. Juslin N, Wirth BD. Interatomic potentials for simulation of He bubble formation in W. J Nucl Mater. Elsevier B.V.; 2013;432:61–6.

37. Beck DE. A new interatomic potential function for helium. Mol Phys. 1968;14:311–5.

38. Morishita K, Sugano R, Wirth BD, Diaz de la Rubia T. Thermal stability of helium–vacancy

clusters in iron. Nucl Instruments Methods Phys Res Sect B Beam Interact with Mater Atoms. 2003;202:76–81.

39. Yang L, Bergstrom ZJ, Wirth BD. Effect of interatomic potential on the energetics of hydrogen and helium-vacancy complexes in bulk, or near surfaces of tungsten. J Nucl Mater. North-Holland; 2018;512:357–70.

40. Juslin N, Erhart P, Träskelin P, Nord J, Henriksson KOE, Nordlund K, et al. Analytical interatomic potential for modeling nonequilibrium processes in the W–C–H system. J Appl Phys. American Institute of Physics; 2005;98:123520.

41. Plimpton S. Fast parallel algorithms for short-range molecular dynamics. J Comput Phys. 1995;117:1–19; Also see http://lammps.sandia.gov/.

42. Honeycutt JD, Andersen HC. Molecular dynamics study of melting and freezing of small Lennard-Jones clusters. J Phys Chem. American Chemical Society; 1987;91:4950–63.

43. Stukowski A. Visualization and analysis of atomistic simulation data with OVITO–the Open Visualization Tool. Model Simul Mater Sci Eng. 2009;18:015012-1–7; Also see http://www.ovito.org/.

44. Stukowski A. Structure identification methods for atomistic simulations of crystalline materials. Model Simul Mater Sci Eng. 2012;20:045021.

45. Stukowski A. A triangulation-based method to identify dislocations in atomistic models. J Mech Phys Solids. Elsevier; 2014;70:314–9.

46. Hirel P. Atomsk : A tool for manipulating and converting atomic data files ☆. Comput Phys Commun. Elsevier B.V.; 2015;197:212–9.

47. Jiang C, Maloy SA, Srinivasan SG. A computational method to identify interstitial sites in

complex materials. Scr Mater. 2008;58:739–42.

48. Swinburne TD, Ma PW, Dudarev SL. Low temperature diffusivity of self-interstitial defects in tungsten. New J Phys. 2017;19.

49. Swinburne TD, Dudarev SL, Fitzgerald SP, Gilbert MR, Sutton AP. Theory and simulation of the diffusion of kinks on dislocations in bcc metals. Phys Rev B - Condens Matter Mater Phys. 2013;87:1–12.

50. Ventelon L, Willaime F, Leyronnas P. Atomistic simulation of single kinks of screw dislocations in α-Fe. J Nucl Mater. Elsevier B.V.; 2009;386–388:26–9.

51. Frauenfelder R. Solution and Diffusion of Hydrogen in Tungsten. J Vac Sci Technol. 1969;6:388–97.

52. Kimizuka H, Ogata S. Slow diffusion of hydrogen at a screw dislocation core in α-iron. Phys Rev B. American Physical Society; 2011;84:24116.

53. Bombac D, Katzarov IH, Pashov DL, Paxton AT. Theoretical evaluation of the role of crystal defects on local equilibrium and effective diffusivity of hydrogen in iron. Mater Sci Technol. Taylor & Francis; 2017;33:1505–14.

54. Bonny G, Grigorev P, Terentyev D. On the binding of nanometric hydrogen–helium clusters in tungsten. J Phys Condens Matter. 2014;26:485001.